3A.3 EXAMINATION OF THE LINEAR ALGEBRAIC SUBGRID-SCALE STRESS [LASS] MODEL, COMBINED WITH RECONSTRUCTION OF THE SUBFILTER-SCALE STRESS, FOR LARGE-EDDY SIMULATION OF THE NEUTRAL ATMOSPHERIC BOUNDARY LAYER

Rica Mae Enriquez*[1], Fotini Katopodes Chow[2], Robert L. Street[1], Francis L. Ludwig[1]
[1]Stanford University, Stanford, CA
[2]University of California, Berkeley, CA

1. INTRODUCTION

A number of authors have highlighted the features of the atmospheric boundary layer, including coherent structures and anisotropic turbulence (Dubos et al., 2008). Biferale et al. (2004) cite the quantification of anisotropic effects in small-scale turbulence as a theoretical and practical challenge and a first-order question for near-wall large-eddy simulation [LES]. Sullivan et al. (2003) show the anisotropy of turbulence in the Horizontal Array Turbulence Study [HATS] near-ground field data and support the use of mixed subfilter-scale models in LES. Mixed models are useful turbulence models, but a current weakness of the approach is that the subgrid-scale stress model is typically an eddy-viscosity model. Eddy-viscosity models cannot reproduce the observed anisotropy of the normal stresses and, in the simplest forms, cannot support the observed back-scatter of energy.

We are motivated to find the best possible models for the subfilter-scales. Our work (e.g., Chow et al., 2005; Chow and Street, 2009; Ludwig et al., 2009) has used models that combine resolvable subfilter-scale [RSFS] and subgrid-scale [SGS] components in a mixed model for large eddy simulation [LES]. The effectiveness of these models shows them to be useful (Ludwig et al., 2009). Accordingly, we are developing a non-eddy-viscosity SGS model that allows for anisotropy and contains additional physics to improve the mixed model.

2. A NEW MIXED MODEL

We use the Carati et al. (2001) framework for LES, in which we apply a spatial filter [represented here by an overbar] and a discretization filter [wavy overbar]. This produces a subfilter-scale stress [SFS], $\Im_{ij}$, that can be separated into a RSFS stress, B_{ij}, and a SGS stress, A_{ij}:

$$\Im_{ij} = \overline{\widetilde{u_i u_j}} - \bar{\tilde{u}}_i \bar{\tilde{u}}_j = \underbrace{\overline{\widetilde{u_i u_j}} - \overline{\tilde{u}_i \tilde{u}_j}}_{\bar{A}_{ij}} + \underbrace{\overline{\tilde{u}_i \tilde{u}_j} - \bar{\tilde{u}}_i \bar{\tilde{u}}_j}_{B_{ij}} . \tag{1}$$

With this separation, the SFS stress can be parameterized with a mixed model. Here, we choose an algebraic stress model to estimate the SGS stress and we reconstruct the RSFS stress with the approximate deconvolution method of Stolz and Adams (1999), as done by Chow et al. (2005).

* *Corresponding author address*: Rica Mae Enriquez, Stanford University, Civil & Environmental Engineering Department, Stanford, CA, 94305; ricae@stanford.edu

2.1 *The Linear Algebraic Subgrid-Scale Stress [LASS] Model*

The evolution equation for A_{ij} can be designed with a methodology similar to that used by Lilly (1967) and Wyngaard (2004) for SGS stress equations, but with an additional discretization filter operator. This evolution equation includes: advection, diffusion, production, viscosity, pressure redistribution, buoyancy generation, and Coriolis terms. The SGS stress evolution we are modeling is simplified in this work to include only production, dissipation, and pressure redistribution, giving a set of linear algebraic equations; neglected terms are assumed small.

These LASS equations allow normal stress anisotropies near the wall and improve the physical basis compared to eddy-viscosity parameterizations. Production terms need not be modeled, the dissipation term appears in its general isotropic form for high Reynolds number flows, and the pressure redistribution term is replaced with the Launder et al. (1975) model, represented as Π_{ij}, in the LASS model:

$$0 = -\bar{A}_{jk}\frac{\partial \bar{\tilde{u}}_i}{\partial x_k} - \bar{A}_{ik}\frac{\partial \bar{\tilde{u}}_j}{\partial x_k} - \tfrac{2}{3}\bar{\varepsilon}\delta_{ij} + \Pi_{ij} . \tag{2}$$

Pressure redistribution, Π_{ij}, is qualitatively broken into ϕ_1, the slow pressure-strain term, ϕ_2, the rapid pressure-strain term, and ϕ_w, the term involving wall effects of ϕ_1 and ϕ_2. Π_{ij} and its accompanying terms are:

$$\begin{aligned}\Pi_{ij} = & \underbrace{- c_1 \frac{\bar{\varepsilon}}{\bar{e}}\left(\bar{A}_{ij} - \frac{2}{3}\bar{e}\delta_{ij}\right)}_{\text{Slow Pressure-Strain, } \phi_1} \\ & \underbrace{- c_2\left(P_{ij} - \frac{2}{3}P\delta_{ij}\right) - c_3\bar{e}\bar{\tilde{S}}_{ij} - c_4\left(D_{ij} - \frac{2}{3}P\delta_{ij}\right)}_{\text{Rapid Pressure-Strain, } \phi_2} \\ & \underbrace{+\left(c_5\frac{\bar{\varepsilon}}{\bar{e}}(\bar{A}_{ij} - \frac{2}{3}\bar{e}\delta_{ij}) + c_6 P_{ij} - c_7 D_{ij} + c_8\bar{e}\bar{\tilde{S}}_{ij}\right) f(z)}_{\text{Wall Effects, } \phi_w} ,\end{aligned} \tag{3}$$

$$P_{ij} = -\bar{A}_{ik}\frac{\partial \bar{\tilde{u}}_j}{\partial x_k} - \bar{A}_{jk}\frac{\partial \bar{\tilde{u}}_i}{\partial x_k} , \tag{4}$$

$$D_{ij} = -\bar{A}_{ik}\frac{\partial \bar{\tilde{u}}_k}{\partial x_j} - \bar{A}_{jk}\frac{\partial \bar{\tilde{u}}_k}{\partial x_i} , \tag{5}$$

$$f(z) = \begin{cases} 0.2\dfrac{\Delta_g}{z} & \text{if } z < z_c, \\ 0 & \text{if } z \geq z_c \end{cases}, \text{ and} \tag{6}$$

f(z) is a wall function from Launder et al. (1975) that relates the dissipation length scale with distance from the wall. The dissipation length scale, $\bar{e}^{3/2}\bar{\varepsilon}^{-1}$, simplifies to $\Delta_g = \left(\Delta_x \Delta_y \Delta_z\right)^{1/3}$ because we choose $\bar{\varepsilon} = 1.12\bar{e}^{3/2}\Delta_g^{-1}$ (Yoshizawa, 1986). We use the Advanced Regional Prediction System [ARPS] as our ABL code, and the ARPS tuburblent kinetic energy]TKE] transport equation provides values of $\bar{e}$, the TKE, needed in the LASS. ARPS TKE is based on 1.5-TKE closure models of Deardorff (1980) and Moeng (1984). We placed a cap on the wall function at the height of $z_c = 4\Delta x = 128$ m because wall effects should be minimal above this height.

Table 1. LASS model coefficients

c_1	c_2	c_3	c_4	c_5	c_6	c_7	c_8
1.8	0.78	0.27	0.22	0.8	0.06	0.06	0.0

Model coefficients [Table 1] are based on suggestions from Launder et al. (1975), Morris (1984), Shabbir and Shih (1992), and Wallin and Johansson (2000).

Enriquez et al. (2010) carried out a comparison of the LASS, Smagorinsky, and dynamic Wong-Lilly [DWL] models. The Smagorinsky and DWL models are eddy-viscosity SGS stress models, which are discussed in our previous work (Chow et al., 2005; Chow and Street, 2009; Ludwig et al., 2009). While in many ways comparable to the DWL model and superior to the Smagorinsky model, the LASS model correctly represents normal stress anisotropy near the ground [see section 4.3].

2.2 *LASS with Reconstruction of the Subfilter-scale Stress*

We examine the performance of the combination of the LASS model to parameterize the SGS stress, A_{ij}, and reconstruction of the SFS stress, B_{ij}. The integration of eddy-viscosity parameterizations of A_{ij} and reconstruction of B_{ij} has been studied previously (Gullbrand and Chow, 2003; Chow et al., 2005; Chow and Street, 2009; Ludwig et al., 2009) with the Dynamic Reconstruction Model of Chow et al. (2005), which applies the DWL model for the SGS stress and the approximate deconvolution model [ADM] of Stolz and Adams (1999) for the SFS stress.

B_{ij} is reconstructed by using the ADM, in which an approximate unfiltered velocity, $\tilde{u}_i^*$, is reclaimed using van Cittert's (1931) iterative approach:

$$\tilde{u}_i^* = \bar{\tilde{u}}_i + (I-G)*\bar{\tilde{u}}_i + (I-G)*\left[(I-G)*\bar{\tilde{u}}_i\right] + \ldots, \tag{7}$$

where I is the identity operation and G is the explicit spatial filter. B_{ij} is then calculated with $\tilde{u}_i^*$ and by applications of the appropriate filters by following the equation $B_{ij} = \overline{\widetilde{u_i^* u_j^*}} - \bar{\tilde{u}}_i^* \bar{\tilde{u}}_j^*$. The reconstruction level [ADM0, ADM1, etc.] depends on the truncation of the unfiltered velocity equation. Level n means that n+1 terms of the series are retained. At the zeroth order [ADM0], B_{ij} reduces to the Bardina scale-similarity case.

Here, we assess the performance of LASS with three different levels of reconstruction [LASS-ADM0, LASS-ADM1, and LASS-ADM5] in a neutral boundary layer flow.

3. NEUTRAL BOUNDARY LAYER FLOW LES SETUP

The Advanced Regional Prediction System [ARPS] is 3D, compressible, non-hydrostatic, parallelized, and appropriate for LES (Doyle et al., 2000; Xue et al., 2000; Xue et al., 2001; Chow et al., 2005). We test the performance of the LASS model with different levels of reconstruction with ARPS by simulating the rotation-influenced neutral boundary layer [NBL] used by others (Andren et al., 1994; Sullivan et al., 1994; Kosović, 1997; Porté-Agel et al., 2000; Chow et al., 2005; Ludwig et al., 2009, and others) to investigate a fully turbulent flow. Table 2 summarizes parameters used here. After thirty non-dimensional time periods [30 tf = 300,000 s], the flow has reached quasi-steady state for the mean velocities.

Table 2. Neutral boundary layer LES parameters

Horizontal resolution, Δ_x	32 m
Vertical resolution	37.5 m average, 10 m minimum
Domain height, H	1500 m
Wall function top, z_c	$4\Delta_x$
Domain size	1.28 km x 1.28 km x 1.5 km
Geostrophic wind	[Ug, Vg] = [10, 0] m s^{-1}
Coriolis parameter	f [45° N] = 1 x 10^{-4} s^{-1}
Lateral boundaries	Periodic
Bottom boundary	Rigid wall, semi-slip
Roughness length	0.1 m

Data from an 8 m horizontal and 2.5 m minimum vertical resolution NBL simulation is also used for some analysis. For differences in the setup, see Ludwig et al. (2009).

4. LES RESULTS

The following section discusses the parameters examined to assess the performance of the LASS model with different levels of reconstruction. Each parameter is sampled at a distinct interval and within differing time spans. We use Ludwig et al. (2009) for guidance. Please see Table 3 for details.

Table 3. Sampling interval, time span, and method of averaging

	Sample Interval	Time Span
Logarithmic velocity profiles	5,000 s	200,000–300,000 s
Resolved/reconstructed vertical velocity	2,500 s	260,000–280,000 s
Forward-, backward-scatter	1,000 s	260,000–280,000 s
1D energy spectra at z/H ~ 0.07	1,000 s	200,000–300,000 s
SGS anisotropy, 8 m horizontal resolution	500 s	134,000–142,500 s

Each variable is averaged horizontally and in time, except for the instantaneous vertical velocity snapshots.

4.1 *Logarithmic Velocity Profiles*

The turbulent Ekman layer should follow a logarithmic law up to about 10% of the boundary layer depth (Blackadar and Tennekes, 1968). The mean velocity normalized by the friction velocity, u_*, versus height for simulations using the Smagorinsky, LASS, LASS-ADM0, LASS-ADM1, and LASS-ADM5 models is displayed in Figure1a. The non-dimensional velocity gradient, Φ_M, defined as

$$\Phi_M = \frac{\kappa z}{u_*}\sqrt{\left(\frac{\partial\langle\bar{\tilde{u}}\rangle}{\partial z}\right)^2 + \left(\frac{\partial\langle\bar{\tilde{v}}\rangle}{\partial z}\right)^2}, \qquad (8)$$

is a more sensitive measure of how a model adheres to the logarithmic law. The von Karman constant, κ, is 0.4. We expect $\Phi_M = 1$ for the logarithmic region, which is within the first 150 m or so above the ground (Sullivan et al., 1994). Smoothed profiles of Φ_M (see Chow et al., 2005) are shown in Figure 1b. The Φ_M profile of the Smagorinsky model, with a maximum Φ_M is 1.6 near the surface, is included as a reminder of the LASS model's great improvement with regard to this parameter (Enriquez et al., 2010). The LASS Φ_M values are about 1.1 near the wall. Reconstruction of the SFS stress slightly improves the profiles; LASS-ADM1 and LASS-ADM5 exhibit Φ_M values near 1.05.

4.2 *Instantaneous Vertical Velocity*

Differences in the vertical velocity patterns are most distinct in the near-wall region and so we show nine snapshots of the resolved vertical velocity patterns from the Smagorinsky and LASS simulations and reconstructed vertical velocity snapshots from LASS-ADM5 simulations at 15 m in Figure 2. As a reminder, reconstructed velocities re-introduce SFS wavenumbers and are intended to provide more accurate approximations of the velocity.

Structure size differs between simulations using varying turbulence models because the interface area for transfer of momentum may adapt to these "viscosity" changes (Ludwig et al., 2009). The results from the Smagorinsky model have much larger structures than the other two simulation results. Ludwig et al. (2009) discuss how the larger eddy viscosities of traditional eddy-viscosity models "... produce smoother large-scale structures with less interfacial area and intricacy." The smaller resolved scales observed in the results from the LASS and LASS-ADM5 model data compared to Smagorinsky model results may be due to incorporation of more physics. The reconstructed vertical velocity from

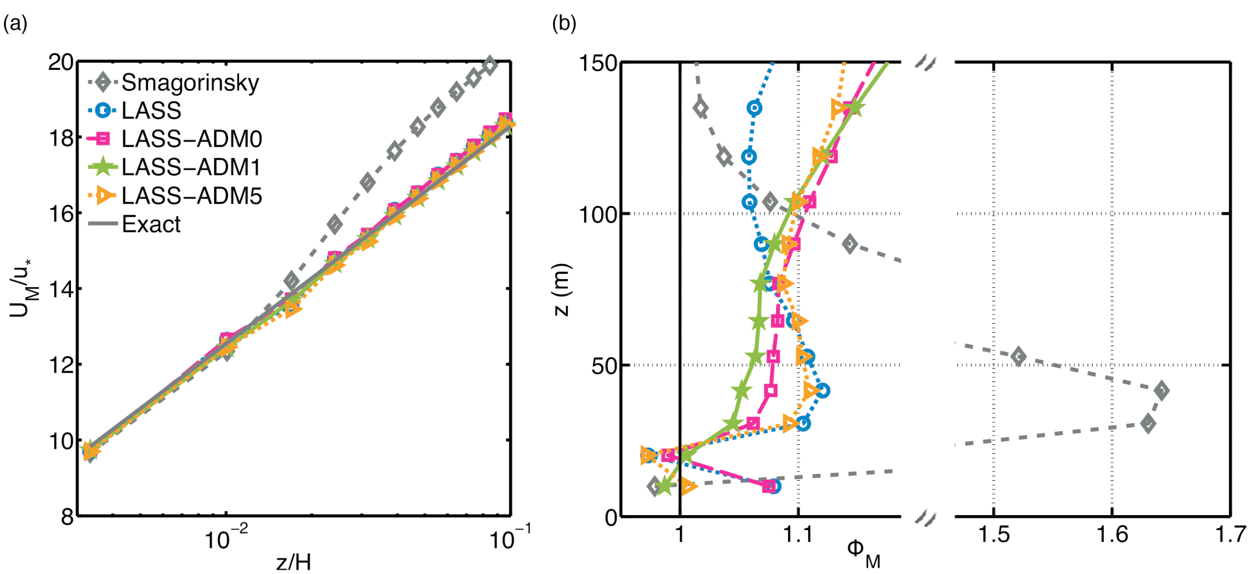

Figure 1. Comparison of (a) normalized mean wind speed and (b) non-dimensional mean shear, Φ_M, profiles for the Smagorinsky, LASS, LASS-ADM0, LASS-ADM1, and LASS-ADM5 models with the exact logarithmic velocity law.

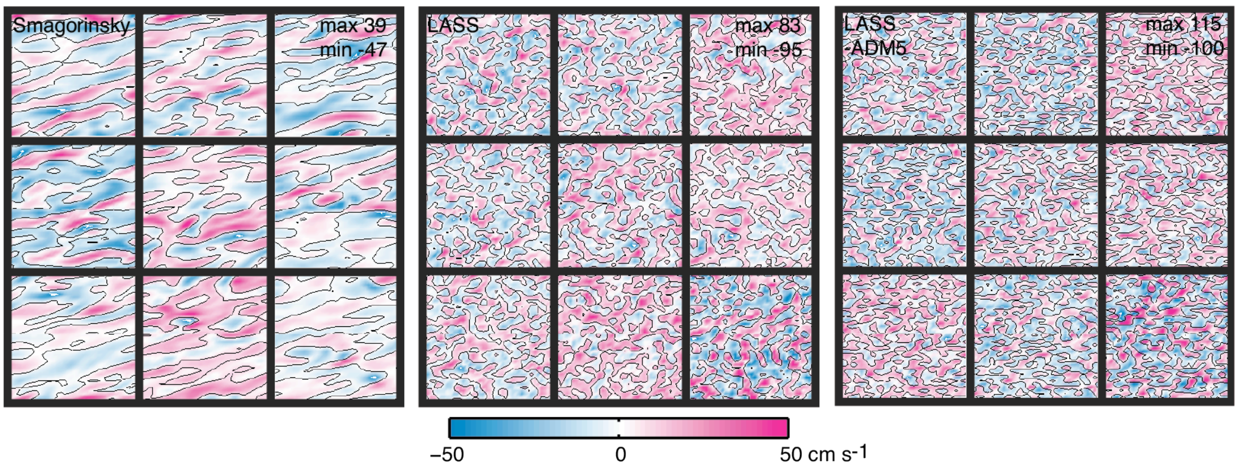

Figure 2. Resolved [Smagorinsky and LASS models] and reconstructed [LASS-ADM5] vertical velocity snapshots at 15 m with black contour lines of w = 0 cm s^{-1}. Snapshots are every 2,500 s from 260,000 s to 280,000 s, and are placed left to right and then top to bottom. Extreme values [cm s^{-1}] are shown in each model square corner.

LASS-ADM5 simulations also provides more physics than resolved vertical velocity of LASS simulation results; its snapshots appear to have smaller structures than the LASS model simulation plot.

4.3 ***SGS Anisotropy***

Contrary to the typical assumption of SGS stress isotropy, SGS normal stresses are anisotropic near walls. Here, SGS stress anisotropy, $\sigma_{ij} = A_{ij} - 1/3A_{kk}$ is normalized by u_*^2 in our plot. For an appropriate comparison with values from the Horizontal Array Turbulence Study [HATS], we assess the SGS anisotropy from an 8 m horizontal and 2.5 m minimum vertical resolution case [Figure 3]. The x and y coordinates at each level have been rotated to be parallel and perpendicular to, respectively, the local mean velocity to be consistent with the HATS data analysis. The HATS data are for a moderately convective case, but at 6 m, the stability parameter [-z/L] is small so shear-driven turbulence dominates and deviations from neutral-stability results are small.

The LASS model provides SGS anisotropy in the near-wall and closely mimics the HATS values at 6 m. The cross-stream component demonstrated the largest discrepancy with the HATS data. Interestingly, that component of the HATS data has shown the least agreement with other SGS turbulence models as well (Chen et al., 2009).

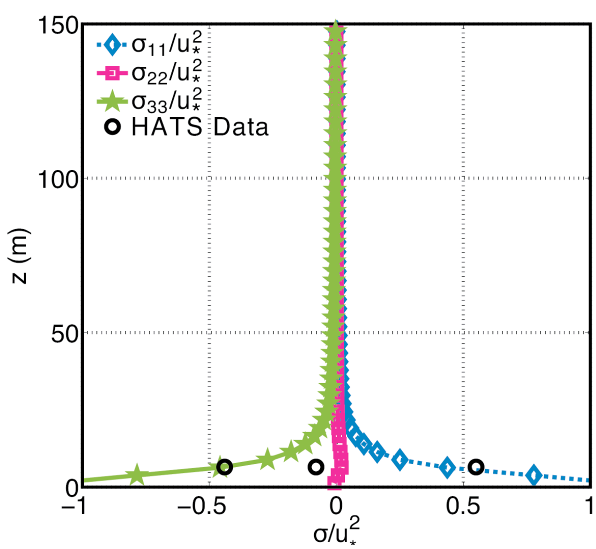

Figure 3. Normalized SGS anisotropies of LASS and experimental Horizontal Array Turbulence Study data (Chen et al., 2009) for an 8 m horizontal resolution simulation.

4.4 ***Forward-Scatter & Back-Scatter***

As seen in atmospheric measurements, back-scatter of energy from smaller scales to larger scales is present near the surface and should be included in an LES turbulence closure scheme (see Porté-Agel et al., 2001; Sullivan et al., 2003; Carper and Porté-Agel, 2004). Some turbulence models have been designed to include backscatter because it may provide a more accurate representation of the development of perturbations (Piomelli et al., 1991).

In LES, forward-scatter represents removal of energy from the resolved scales by the SFS/SGS production terms and that transfer may be or may not be equal to the actual dissipation; back-scatter represents transfer from the SFS/SGS scales back to the resolved scales. Often the SGS/SFS production terms are inaccurately called dissipation terms.

The current form of the LASS model is not designed to allow for back-scatter because the SGS stress evolution equation it is modeling only includes production, dissipation, and pressure redistribution terms. The analogous TKE equation would only include

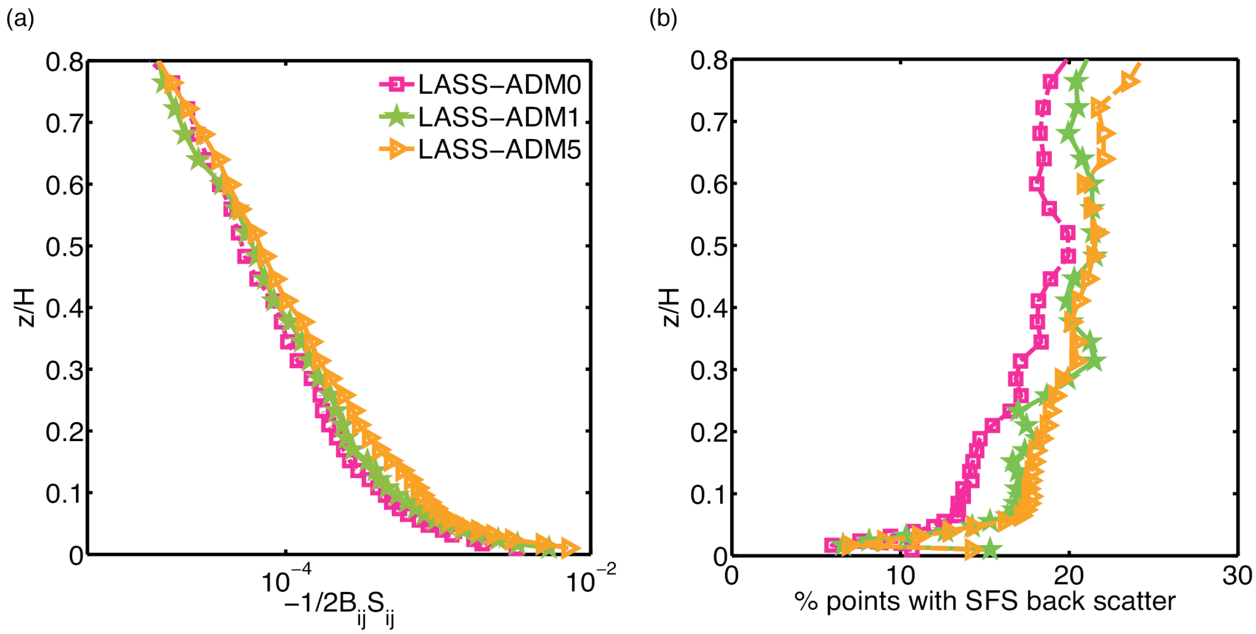

Figure 4. (a) SFS mean forward-scatter of the LASS-ADM0, LASS-ADM1, and LASS-ADM5 simulations as a function of z/H. (b) The percent of back-scatter occurrences at a given z/H for each horizontal plane and all time samples.

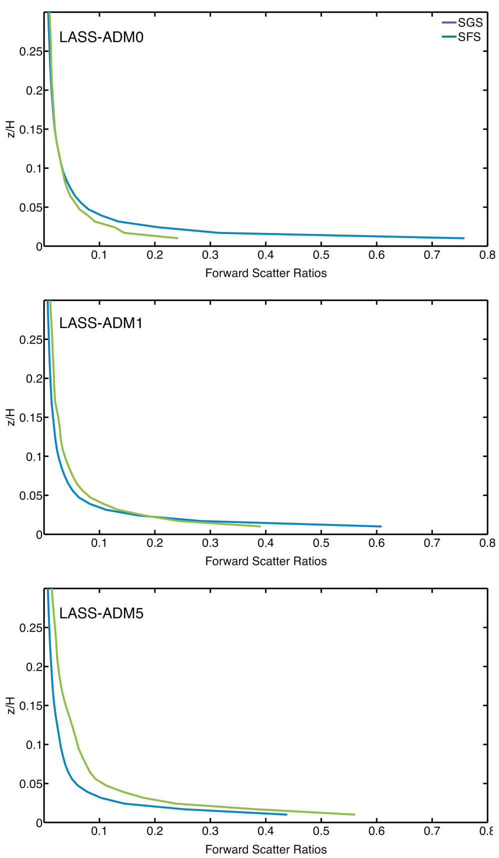

Figure 5. Ratios of SGS and SFS mean forward-scatter and maximum total forward-scatter of the LASS-ADM0, LASS-ADM1, and LASS-ADM5 simulations as a function of z/H.

production and dissipation terms since pressure redistribution terms drop out. The LASS model does allow the SGS stress, A_{ij}, and the deformation tensor, S_{ij}, to have opposite signs, but at a specific point the production term, $-1/2A_{ij}S_{ij}$, must exactly balance the computed dissipation as defined in Sec. 2.1; thus, for the current version of LASS, production does equal dissipation and so only forward-scatter of energy from resolved scales to SGS scales is allowed.

The fact that we have this SGS TKE production and dissipation balance and promising results confirms previous observations. Moser et al. (1999) anticipate that TKE production and dissipation will be balanced for the log region of high Reynolds number channel flows. In addition, Charuchittipan and Wilson (2009) find that a local equilibrium between TKE production and dissipation is a good approximation for the neutral boundary layer.

In the near future we will include more terms in the LASS SGS stress evolution equation, e.g., advection, diffusion, and buoyancy, in order to provide the potential for back-scatter events in the LASS model. Wyngaard (2004) noted that models such as LASS “could give” backscatter. The addition of reconstruction has been shown to allow for back-scatter, and we will examine here how different levels of reconstruction affect back-scatter and forward-scatter.

The LASS model with varying levels of reconstruction provide a mean SFS forward-scatter, $-1/2B_{ij}S_{ij}$, as seen in Figure 4a. Figure 4b shows that the level of back-scatter events are ~20% for the LASS-ADM0, LASS-ADM1, and LASS-ADM5 models (cf., Piomelli et al., 1991). There is a general increase of back-scatter events from LASS-ADM0 to LASS-ADM1,

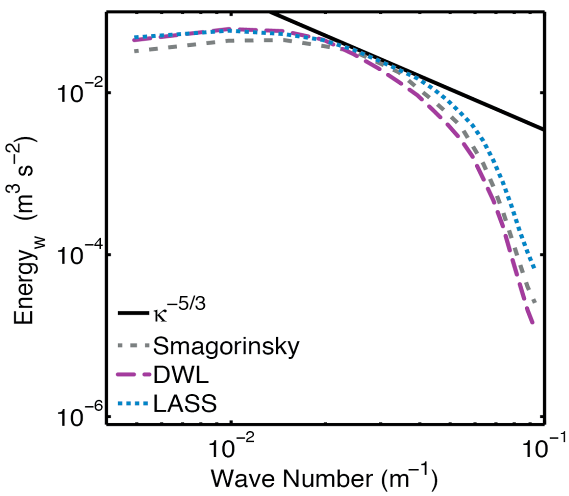

Figure 6. 1D energy spectra of resolved vertical velocities at z/H ~ 0.07 for the Smagorinsky, dynamic Wong-Lilly [DWL], and LASS simulations.

but the level of back-scatter events for LASS-ADM5 is similar to that of LASS-ADM1.

The maximum total forward scatter is near the surface. The SGS provides ~80% of this near-surface forward-scatter for LASS-ADM0 [Figure 5]. With increasing levels of reconstruction, the SGS provides less near-surface forward-scatter, e.g., the SGS forward-scatter accounts for ~40% of all forward-scatter. With higher levels of reconstruction, there is a larger contribution from the SFS reconstruction and there is less of a burden on the LASS model for an accurate parameterization. The validity and implications of this trend need further examination.

4.5 *Energy Spectra*

Figure 6 shows LASS, Smagorinsky and DWL simulation spectra for the resolved vertical velocity. Comparison of the Smagorinsky and LASS simulation spectra confirms that the LASS model allows more small-scale energy, reflecting the filtering effect of the the Smagorinsky model on small scales. We speculate that the reduced small scale energy [high wave number] in the DWL spectra also reflects filtering, but in this case it is done by the DWL test filter.

Consider a schematic of an LES energy spectra in the Carati et al. (2001) context [Figure 7a]. The two components of turbulence are the RSFS and the SGS. We deal with these two pieces when calculating the total Reynolds stress. The RSFS is partly reconstructed*

* The RSFS region contains numerical error [NE] because there is a modified wavenumber effect on calculating derivatives with a finite-difference scheme (Moin, 2001).

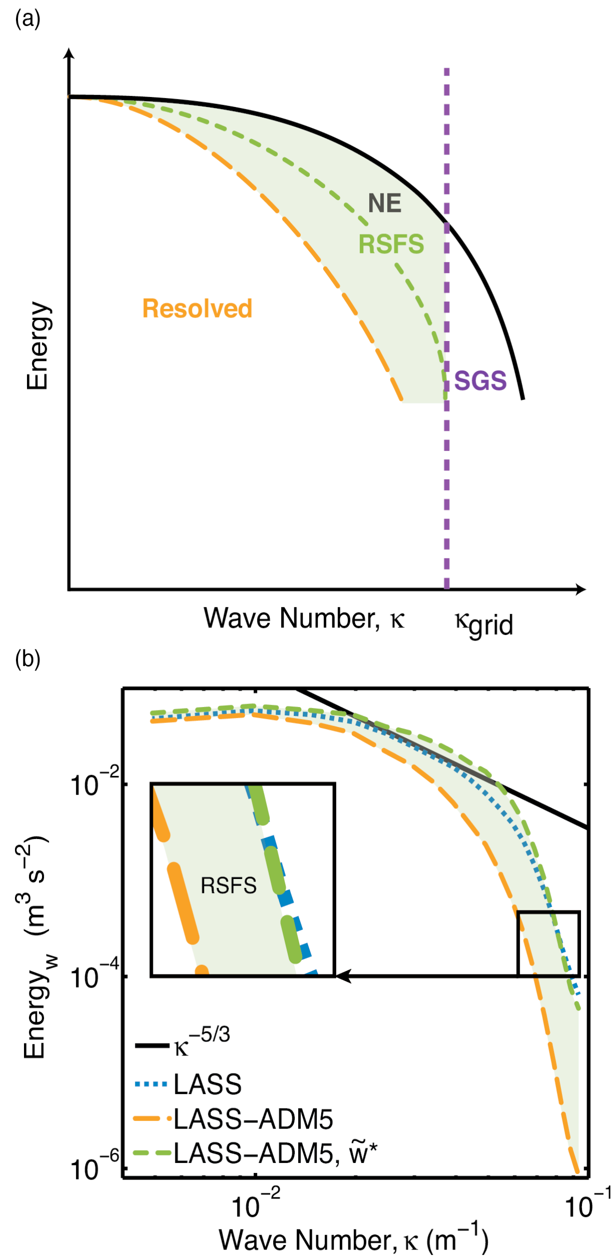

Figure 7. (a) Schematic of energy spectra components as adapted from Carati et al. (2001) and Chow et al. (2005). (b) 1D energy spectra at z/H ~ 0.07 for resolved vertical velocities of LASS and LASS-ADM5 simulations, and for the reconstructed vertical velocity of a LASS-ADM5 simulation. A resolved subfilter-scale region can be clearly seen.

from the resolved velocities, and the SGS is modeled by LASS.

Ludwig et al. (2009) observed that models with energy back-scatter better mimic the expected interactions between resolved and subfilter scales, yielding more active spectra at smaller scales [higher wave numbers] in the resolved flows. This can be seen by comparing the one-dimensional energy spectra of the resolved and reconstructed vertical velocity, $\tilde{w}^*$, for the LASS-ADM5 simulation depicted in Figure 7b. [$\tilde{w}^*$ is not the vertical velocity scale.] The difference in the spectra shows that there is a RSFS region. Comparisons of the LASS-ADM5 and the LASS spectra show that 1) they are significantly different and 2) reconstruction of the SFS stress has indeed distributed more energy to the SFS range. Which is the 'correct' spectrum is ambiguous, but with higher levels of reconstruction, we reduce the numerical error and get a better estimate of the actual velocity than is possible without the reconstruction.

5. CONCLUSIONS

We have shown previously that the LASS model is a more physically complete SGS turbulence model that provides near-wall anisotropies that eddy-viscosity models do not. Here, we have shown that a mixed model that incorporates LASS and reconstruction of the SFS stress further improves adherence to the log law and provides backscatter for the neutral boundary layer.

From the work presented here, we realized that a resolution study for this new mixed model would be enlightening (see Bryan et al., 2003 for an example) and plan to carry this forward soon. In addition, we are currently creating a Generalized LASS model [GLASS], that will include coupled equations for SGS flux/stress components of heat, water vapor, and momentum.

6. ACKNOWLEDGMENTS

We appreciate the support from an NSF Graduate Research Fellowship [RME], NSF Grant ATM-0453595, and NCAR for the computing time used in this research and for support [RME & RLS] through the Advanced Study Program.

7. REFERENCES

Andren, A., A. R. Brown, P. J. Mason, J. Graf, U. Schumann, C. H. Moeng, and F. T. M. Nieuwstadt, 1994: Large-eddy simulation of a neutrally stratified boundary layer: A comparison of four computer codes. *Q. J. Roy. Meteor. Soc.*, **120,** 1457-1484.

Biferale, L., I. Daumont, A. Lanotte, and F. Toschi, 2004: Theoretical and numerical study of highly anisotropic turbulent flows. *Eur. J. Mech. B-Fluid*, **23,** 401-414.

Blackadar, A. K., and H. Tennekes, 1968: Asymptotic similarity in neutral barotropic planetary boundary layers. *J. Atmos. Sci.*, **25,** 1015-1020.

Bryan, G. H., J. C. Wyngaard, and J. M. Fritsch, 2003: Resolution requirements for the simulation of deep moist convection. *Mon. Weather Rev.*, **131,** 2394-2416.

Carati, D., G. S. Winckelmans, and H. Jeanmart, 2001: On the modelling of the subgrid-scale and filtered-scale stress tensors in large-eddy simulation. *J. Fluid Mech.*, **441,** 119-138.

Carper, M. A., and F. Porté-Agel, 2004: The role of coherent structures in subfilter-scale dissipation of turbulence measured in the atmospheric surface layer. *Journal of Turbulence*, **5,** N40.

Charuchittipan, D., and J. Wilson, 2009: Turbulent kinetic energy dissipation in the surface layer. *Bound.-Lay. Meteorol.*, **132,** 193-204.

Chen, Q., M. J. Otte, P. P. Sullivan, and C. Tong, 2009: A posteriori subgrid-scale model tests based on the conditional means of subgrid-scale stress and its production rate. *J. Fluid Mech.*, **626,** 149-181.

Chow, F. K., R. L. Street, M. Xue, and J. H. Ferziger, 2005: Explicit filtering and reconstruction turbulence modeling for large-eddy simulation of neutral boundary layer flow. *J. Atmos. Sci.*, **62,** 2058-2077.

Chow, F. K., and R. L. Street, 2009: Evaluation of turbulence closure models for large-eddy simulation over complex terrain: Flow over Askervein Hill. *J. Appl. Meteorol. Clim.*, **48,** 1050-1065.

Deardorff, J. W., 1980: Stratocumulus-capped mixed layers derived from a three-dimensional model. *Bound.-Lay. Meteorol.*, **18,** 495-527.

Doyle, J. D., D. R. Durran, C. Chen, B. A. Colle, M. Georgelin, V. Grubisic, W. R. Hsu, C. Y. Huang, D. Landau, Y. L. Lin, G. S. Poulos, W. Y. Sun, D. B. Weber, M. G. Wurtele, and M. Xue, 2000: An intercomparison of model-predicted wave breaking for the 11 January 1972 Boulder windstorm. *Mon. Weather Rev.*, **128,** 901-914.

Dubos, T., P. Drobinski, and P. Carlotti, 2008: Turbulence anisotropy carried by streaks in the neutral atmospheric surface layer. *J. Atmos. Sci.*, **65,** 2631-2645.

Enriquez, R. M., R. L. Street, and F. L. Ludwig, 2010 of Conference: Algebraic subgrid-scale turbulence modeling in large-eddy simulation of the atmospheric boundary layer. The 5th International Symposium on Computational Wind Engineering, Chapel Hill, NC, International Association for Wind Engineering, Paper 154, 8 pp.

Gullbrand, J., and F. K. Chow, 2003: The effect of numerical errors and turbulence models in large-eddy simulations of channel flow, with and without explicit filtering. *J. Fluid Mech.*, **495,** 323-341.

Kosović, B., 1997: Subgrid-scale modelling for the large-eddy simulation of high-Reynolds-number boundary layers. *J. Fluid Mech.*, **336,** 151-182.

Launder, B. E., G. J. Reece, and W. Rodi, 1975: Progress in the development of a Reynolds-stress turbulence closure. *J. Fluid Mech.*, **68,** 537-566.

Lilly, D. K., 1967: The representation of small-scale turbulence in numerical simulation experiments. *IBM Scientific Computing Symposium on Environmental Sciences, IBM Form No. 320-1951*, 195-210 pp.

Ludwig, F. L., F. K. Chow, and R. L. Street, 2009: Effect of turbulence models and spatial resolution on resolved velocity structure and momentum fluxes in large-eddy simulations of neutral boundary layer flow. *J. Appl. Meteorol. Clim.*, **48,** 1161-1180.

Moeng, C.-H., 1984: A large-eddy-simulation model for the study of planetary boundary-layer turbulence. *J. Atmos. Sci.*, **41,** 2052-2062.

Moin, P., 2001: *Fundamentals of engineering numerical analysis.* Cambridge University Press, 224 pp.

Morris, P. J., 1984: Modeling the pressure redistribution terms. *Phys. Fluids*, **27,** 1620-1623.

Moser, R. D., J. Kim, and N. N. Mansour, 1999: Direct numerical simulation of turbulent channel flow up to re[sub tau] = 590. *Phys. Fluids*, **11,** 943-945.

Piomelli, U., W. H. Cabot, P. Moin, and S. Lee, 1991: Subgrid-scale backscatter in turbulent and transitional flows. *Phys. Fluids A*, **3,** 1766-1771.

Porté-Agel, F., C. Meneveau, and M. B. Parlange, 2000: A scale-dependent dynamic model for large-eddy simulation: Application to a neutral atmospheric boundary layer. *J. Fluid Mech.*, **415,** 261-284.

Porté-Agel, F., M. B. Parlange, C. Meneveau, and W. E. Eichinger, 2001: A priori field study of the subgrid-scale heat fluxes and dissipation in the atmospheric surface layer. *J. Atmos. Sci.*, **58,** 2673-2698.

Shabbir, A., and T. H. Shih, 1992: Critical assessment of Reynolds stress turbulence models using homogeneous flows. NASA TM 105954I, COMP-92-24, CMOTT-92-12.

Stolz, S., and N. A. Adams, 1999: An approximate deconvolution procedure for large-eddy simulation. *Phys. Fluids*, **11,** 1699-1701.

Sullivan, P. P., J. C. McWilliams, and C.-H. Moeng, 1994: A subgrid-scale model for large-eddy simulation of planetary boundary-layer flows. *Bound.-Lay. Meteorol.*, **71,** 247-276.

Sullivan, P. P., T. W. Horst, D. H. Lenschow, C.-H. Moeng, and J. C. Weil, 2003: Structure of subfilter-scale fluxes in the atmospheric surface layer with application to large-eddy simulation modelling. *J. Fluid Mech.*, **482,** 101-139.

Van Cittert, P., 1931: Zum einfluß der spaltbreite auf die intensitätsverteilung in spektrallinien II. *Zeitschrift für Physik* **69,** 298-308.

Wallin, S., and A. V. Johansson, 2000: An explicit algebraic Reynolds stress model for incompressible and compressible turbulent flows. *J. Fluid Mech.*, **403,** 89-132.

Wyngaard, J. C., 2004: Toward numerical modeling in the `terra incognita'. *J. Atmos. Sci.*, **61,** 1816-1826.

Xue, M., K. K. Droegemeier, and V. Wong, 2000: The Advanced Regional Prediction System (ARPS) - A multi-scale nonhydrostatic atmospheric simulation and prediction model. Part I: Model dynamics and verification. *Meteorol. Atmos. Phys.*, **75,** 161-193.

Xue, M., K. K. Droegemeier, V. Wong, A. Shapiro, K. Brewster, F. Carr, D. Weber, Y. Liu, and D. Wang, 2001: The Advanced Regional Prediction System (ARPS) - A multi-scale nonhydrostatic atmospheric simulation and prediction tool. Part II: Model physics and applications. *Meteorol. Atmos. Phys.*, **76,** 143-165.

Yoshizawa, A., 1986: Statistical theory for compressible turbulent shear flows, with the application to subgrid modeling. *Phys. Fluids*, **29,** 2152-2164.